

IMPROVEMENT OF SYNCHRONOUS AND ASYNCHRONOUS MOTOR DRIVE SYSTEMS SUPPLIED BY PHOTOVOLTAIC ARRAYS WITH FREQUENCY CONTROL

Laid Zarour — Rachid Chenni —
Abdelhalim Borni — Aissa Bouzid *

The dynamic performances of a permanent magnet synchronous motor (PMSM) and an asynchronous motor (ASM) connected to a photovoltaic (PV) array through an inverter are analyzed. The mathematical models of PV array, inverter/motor and controller are developed. The photovoltaic array is represented by an equivalent circuit whose parameters are computed using experimentally determined current-voltage ($I - V$) characteristics. The necessary computer algorithm is developed to analyze the performance under different conditions of the solar illumination for a pump load. The study also examines the effectiveness of the drive system both for starting and DC link voltage fluctuations caused by varying solar illumination.

Key words: solar energy, optimization, photovoltaic arrays, pumping, modelling, efficiency

1 INTRODUCTION

Several authors lent much attention to the study of the dynamic performance of the photovoltaic pumping systems. Appelbaum and Bany [1] analyzed the performance of a direct motor with separate excitation fed by a photovoltaic generator. Later, Appelbaum [2] studied the dynamic behaviour of a photovoltaic panel associated directly with a DC motor with excitation series. Roger [3] showed that a load such centrifugal pump, driven by a DC motor, represents a load matched to the characteristics of PV generator. In a former work, the dynamic performance of a PV generator involving a system, permanent magnet motor associate at a centrifugal pump, was studied by Anis and Metwally [4]. Recently Betka [5] presented the performance optimization of an asynchronous motor associated at a PV generator.

In this work, the dynamic performance of a system which uses, once a synchronous motor with permanent magnet and another time an asynchronous motor, is studied. For this last type of engine, the primary current and flux changes in accordance with the changes in the applied voltage. It is not the case with the permanent magnet synchronous motor where flux is constant. The electric model of the system is simulated using the software MATLAB 6p5 for various solar illuminations and temperatures

2 ELECTRICAL MODEL FOR A PHOTOVOLTAIC CELL

The electrical model of a solar cell is composed of a diode, two resistances and a current generator [6], [7],

[8]. The relationship between the voltage V (V) and the current I (A) is given by

$$I = I_L - I_0 \left(\exp \frac{V + R_S I}{A} - 1 \right) - \frac{V + R_S I}{R_P}, \quad (1)$$

where I_L , I_0 and I are the photocurrent, the inverse saturation current and the operating current, R_S and R_P are series and parallel resistances, respectively, which depend on the incident solar radiation and the cell temperature. $A = \frac{KT}{q}$ is the diode quality factor. K and q are Boltzmann constant and electronic charge respectively. Townsend (1989), Eckstein (1990), Al-Ibrahimi (1996), propose the model with four parameters assuming that the parallel resistance is infinite – so (1) can be rewritten as

$$I = I_L - I_0 \left(\exp \frac{V + R_S I}{A} - 1 \right). \quad (2)$$

The current and the voltage parameters of the PV generator are: $I_{pv} = I$ and $V_{pv} = n_s N_s V$, where n_s , N_s are the numbers of series cells in the panel and of the series panels in the generator ($n_s = 36$).

Now only the four parameters I_L , I_0 , R_s and A need to be evaluated, a method to calculate these parameters has been developed by Townsend (1989) and Eckstein (1990), Duffie and Beckman (1991). Since there are four unknown parameters, four conditions of the current I and the voltage V are needed. Generally, available manufacturer's information are set at three points at the reference conditions, $G = 1000 \text{ W/m}^2$ and $T = 25^\circ\text{C}$, the voltage at open circuit $V_{oc,ref}$, the current at short circuit $I_{sc,ref}$ and the maximum power point $V_{mp,ref}$ and $I_{mp,ref}$. The 4th condition comes from the knowledge of the temperature coefficient $\mu_{I_{sc}}$ at short circuit and $\mu_{V_{oc}}$ at open circuit. E_g is the band gap energy (1.12 eV) The following

* Laboratoire d'électrotechnique Faculté des sciences de l'ingénieur Université Mentouri de Constantine, Algérie;
rachid.chenni@caramail.com, laidzarour@hotmail.fr

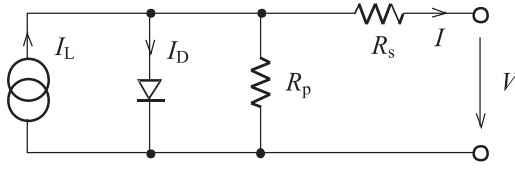


Fig. 1. Equivalent circuit of PV cell

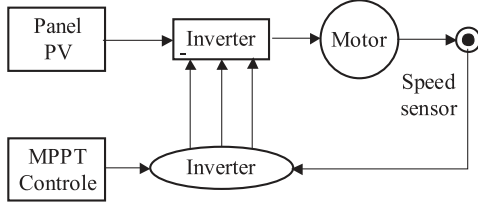


Fig. 2. Block diagram of the global system

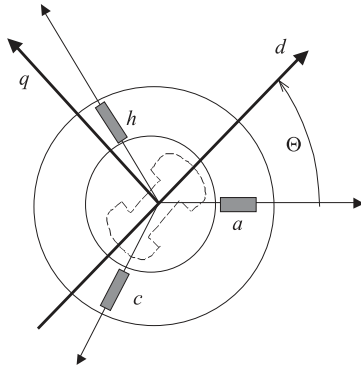


Fig. 3. PMSM three phase model

equations, (3) to (6), are used to calculate the parameters of the photovoltaic cells in a standard condition based on the experimental data.

$$R_{s,ref} = \frac{A_{ref} \ln\left(1 - \frac{I_{mp,ref}}{I_{L,ref}}\right) - V_{mp,ref} + V_{oc,ref}}{I_{mp,ref}}, \quad (3)$$

$$A = \frac{\mu V_{oc} T_{c,ref} - V_{oc,ref} + E_g n_s}{\frac{T_{c,ref} \mu I_{sc}}{I_{L,ref}} - 3}. \quad (4)$$

From equation (2) at reference condition and short circuit point, the diode current I_0 is very small (in the order to 10^{-5} at 10^{-6} A), so the exponential term is neglected.

$$I_{sc,ref} \cong I_{L,ref}, \quad (5)$$

$$I_{0,ref} = \frac{I_{L,ref}}{\exp\left(\frac{V+R_s I}{A}\right) - 1} \quad (6)$$

The indices *oc*, *sc*, *mp* and *ref* refer to the open circuit, the short circuit, the maximum power and the reference condition respectively. The cell parameters change with the solar radiation $G(W/m^2)$ and ambient temperature

$T(^{\circ}K)$ [7] and can be estimated by the following equation. For a given radiation and temperature, the cell parameters are then calculated from

$$T = T_a + \frac{G_T}{G_{T_{noct}}}(T_{noct} - T_a)\left(1 - \frac{\eta_c}{\tau_\alpha}\right), \quad (7)$$

$$I_L = \frac{G}{G_{ref}}\{I_{L,ref} + \mu_{I_{sc}}(T_c - T_{ref})\}, \quad (8)$$

$$I_0 = I_{0,ref}\left(\frac{T}{T_{ref}}\right)^3 \exp\left[\frac{n_s E_g}{A}\left(1 - \frac{T_{c,ref}}{T_c}\right)\right], \quad (9)$$

$$R_s = R_{s,ref}, \quad (10)$$

$$A = A_{ref} \frac{T_c}{T_{c,ref}}. \quad (11)$$

Here, T_a — ambient temperature. η_c — cell efficiency. T_{noct} — nominal operating cell temperature and τ_α — transmittance absorbance product. These four parameters, for ambient conditions, are found from the equations (7) to (11). By injecting these parameters in the equation (2), we obtain $I - V$ characteristics.

PV Array Characteristics:

$N_s = 11$ panels in series GTO136 – 80/2, $AM = 1.5$, $P_m = 80$ W, $V_{oc,ref} = 21.5$ V, $I_{sc} = 4.73$ A, $I_{mp,ref} = 4.25$ A, $V_{mp,ref} = 16.9$ V, $T_{noct} = 45^{\circ}C$, $G_{ref} = 1000$ Watt/ m^2 , $T_{ref} = 298^{\circ}K$. $\mu_{I_{sc}} = 3 \times 10^{-3}$ A/ $^{\circ}C$, $\mu_{V_{oc}} = 82 \times 10^{-3}$ V/ $^{\circ}C$.

3 GLOBAL SYSTEM MODELLING

The decomposition of the total system in elementary blocks is related directly to the physical function of the block.

3.1 PMSM electrical model

The model of the synchronous motor (PMSM) represented by the three fixed stator windings and the permanent magnet rotor is in Fig. 3. The mathematical dynamic model of a PMSMotor can be described by the following equations in a synchronously rotating $d-q$ reference frame (Grellet and Clerc, 1997), [9] where V_d and V_q , L_d and L_q , i_d and i_q are stator voltages, inductances, and currents components in the (d, q) axis respectively; R_a is the stator resistance per phase, Φ_f is the rotor flux linkage due to the rotor permanent magnet frame, and p_p is the number of pole pairs. For a synchronous machine we have $\omega_r = \omega$ (ω — is the electric pulsation). Using the Park transformation, we pass from the real sizes (V_a , V_b , V_c and i_a , i_b , i_c) to their components (V_o , V_d , V_q and (i_o, i_d, i_q)). The Park matrix is expressed by [9]

$$[P(\theta)] = \sqrt{\frac{2}{3}} \begin{bmatrix} \frac{1}{\sqrt{2}} & \cos \theta & -\sin \theta \\ \frac{1}{\sqrt{2}} & \cos(\theta - \frac{2}{3}\pi) & -\sin(\theta - \frac{2}{3}\pi) \\ \frac{1}{\sqrt{2}} & \cos(\theta - \frac{4}{3}\pi) & -\sin(\theta - \frac{4}{3}\pi) \end{bmatrix}, \quad (12)$$

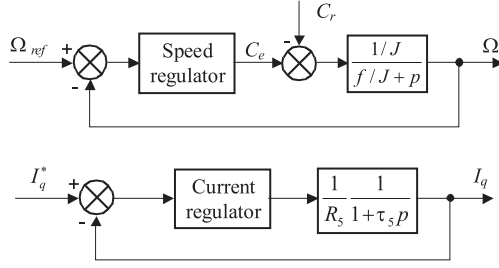


Fig. 4. Block diagram of the speed and current regulators

or in matrix form

$$\begin{bmatrix} V_d \\ V_q \end{bmatrix} = \begin{bmatrix} R_a & -L_q \omega \\ L_d & R_a \end{bmatrix} \begin{bmatrix} i_d \\ i_q \end{bmatrix} + \begin{bmatrix} L_d & 0 \\ 0 & L_q \end{bmatrix} \frac{d}{dt} \begin{bmatrix} i_d \\ i_q \end{bmatrix} + \begin{bmatrix} 0 \\ \Phi_f \omega \end{bmatrix}. \quad (13)$$

Moreover, the PMSM developed electromagnetic torque is given by the following equation

$$C_{em} = \frac{1}{2} [i_s] \left\{ \frac{d}{d\theta_m} [L] \right\} [i_s]. \quad (14)$$

With $\theta_e = \theta_m p_p$, θ_e , θ_m the electrical angle and mechanical respectively, the electromagnetic torque is

$$C_{em} = p_p [(L_d - L_q) i_d + \Phi_f] i_q. \quad (15)$$

For a synchronous machine with smooth poles ($L_d = L_q$), the torque will be $C_{em} = p_p \Phi_f i_q$.

The mechanical equation is written

$$J \frac{d\omega}{dt} + f\omega = C_e - C_r \quad (16)$$

where f and C_r are the friction coefficient and the resistant torque respectively.

PMS Motor Characteristics:

$P = 746$ Watts, $\omega = 188.95$ rad/s, $V = 208$ V, $I_s = 3$ A, $f = 60$ Hz, $I_{sn} = 5$ A, $R_a = 1.93 \Omega$, $L_d = 0.0424$ H, $L_q = 0.00725$ H, $\Psi = 0.003$ Wb, $J = 3 \times 10^{-3}$ Kg/m², $p_p = 2$.

PI parameters:

For speed: $T_i = 0.01$, $K_p = 1$. For current: $T_i = 10$, $K_p = 5$.

3.2 Inverter model

For a three phase equilibrated system, we have: ($V_{an} + V_{bn} + V_{cn} = 0$ and $V_{1m} + V_{2m} + V_{3m} = 3V_{nm}$). In matrix form

$$\begin{bmatrix} V_{an} \\ V_{bn} \\ V_{cn} \end{bmatrix} = \begin{bmatrix} \frac{2}{3} & -\frac{1}{3} & -\frac{1}{3} \\ -\frac{1}{3} & \frac{2}{3} & -\frac{1}{3} \\ -\frac{1}{3} & -\frac{1}{3} & \frac{2}{3} \end{bmatrix} [V_{pv}]. \quad (17)$$

V_{pv} is the photovoltaic generator voltage.

4 VECTORIAL COMMAND PRINCIPLE

From equation (15), the torque control is made on the components of current i_d and i_q . The electromagnetic torque depends only on component i_q . It is maximum for a given current if we impose $i_d = 0$. The obtained torque is then proportional to the current of the machine power supply as in the case of a separately excited DC motor, $C_{em} = p_p \Phi_f i_q$.

5 REGULATORS

To optimize the system with given performances, the system must be controlled. The first role of a regulation system is to oblige the controlled parameters (output of the system) to preserve values as close as possible as those which one chooses like references values. Generally the control devices are with closed loop. For this command, there are three correctors PI used to control the speed and the two components of the stator current. The closed speed loop can be represented by Fig. 4. This transfer function in closed loop has a dynamics of 2nd order.

By identifying the denominator with the canonical form

$$\frac{1}{1 + \frac{2\xi}{\omega_n} p + \frac{p^2}{\omega_n^2}}$$

we obtain

$$\frac{J}{K_i} = \frac{1}{\omega_n^2}, \quad \frac{2\xi}{\omega_n} = \frac{K_p + f}{K_i}. \quad (18,19)$$

6 DESCRIPTION OF THE GLOBAL SYSTEM

Figure 5 represents the total diagram of the vectorial command of a PMSM in a reference mark (d, q). The reference of the forward current I_d^* is fixed at zero and the output of the speed regulator I_q^* constitutes the instruction of the torque. The forward reference currents I_d^* and I_q^* are compared separately with the real currents I_d and I_q of the motor. The errors are applied to the input of the traditional PI regulators. A decoupling block generates the standards reference voltage V_d^* , V_q^* . The system is provided with a regulation speed loop which makes it possible to generate the reference of current I_q^* . This reference is limited to the maximum current. On the other hand, the forward reference current I_d^* is imposed null in our case.

The outputs of the currents regulators I_d and I_q in the reference mark (a, b, c) are used as references of the voltage (V_a^*, V_b^*, V_c^*) for the inverter control which feeds the PMSM.

From the matrix form (13) we pose $U_d = V_d + e_d$, $U_q = V_q + e_q$ and $p = \frac{d}{dt}$ the differential operator.

With $e_d(p) = \omega L_q i_q$ and $e_q(p) = -\omega L_d i_d + \omega \Phi_f$, we can write the following transfer function

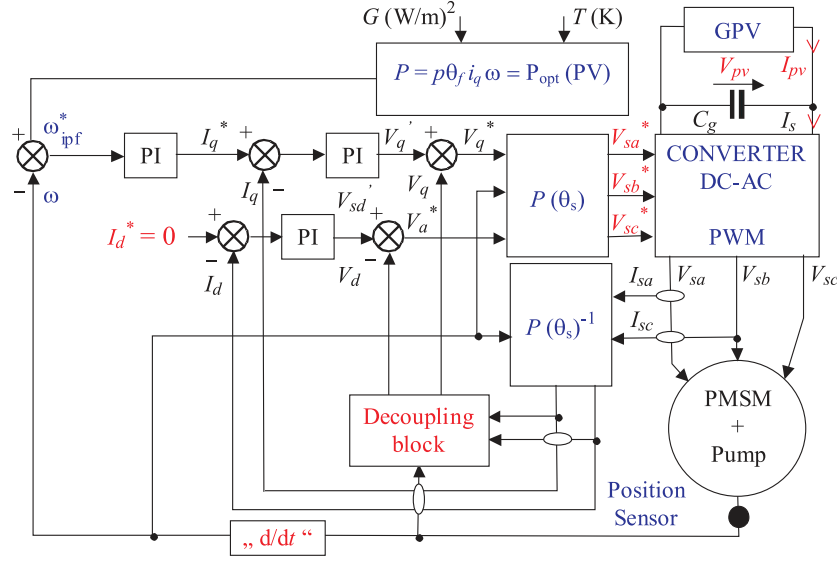


Fig. 5. Block diagram of the PMSM and the GPV

$$F_d(p) = \frac{I_d(p)}{V_q(p) + e_d(p)} = \frac{1}{R_a + pL_d}, \quad (20)$$

$$F_q(p) = \frac{I_q(p)}{V_q(p) + e_q(p)} = \frac{1}{R_a + pL_q}. \quad (21)$$

The compensation causes to uncouple the two axes thanks to a reconstitution in real time from these reciprocal disturbances ($e_d(p)$ and $e_q(p)$). Under such conditions, the system becomes linear, we obtain:

$$V'_q = V_d + \omega L_q i_q = (R_q + pL_d) i_d, \quad (22)$$

$$V'_q = V_q - \omega L_q i_d - \omega \Phi f = (R_q + pL_q) i_q. \quad (23)$$

Therefore the two axes are well uncoupled; the axis d does not depend to any more an axis q . Thus,

$$V_d^* = V'_d - \omega L_q i_q, \quad (24)$$

$$V_q^* = V'_q - \omega L_d i_d + \omega \Phi f. \quad (25)$$

For a damping coefficient, for PMSM, $\xi = 0.7$, and $\omega_n t_{rep} = 3$, t_{rep} representing the response time of speed, the transfer functions for current i_d and current i_q of the system in open loop are respectively, see Fig. 5.

$$H_d(P) = \frac{G_0 C_d(p)}{R_s(1 + \tau_d p)}, \quad (26)$$

$$H_q(P) = \frac{G_0 C_q(p)}{R_s(1 + \tau_q p)} \quad (27)$$

with $\tau_d = \frac{R_s}{L_d}$ and $\tau_q = \frac{R_s}{L_q}$.

The proportional-integral regulators PI ($C_d(p)C_q(p)$), whose transfer functions are given by:

$$C_d(p) = C_q(p) = K(1 + \tau_d p)/p \quad (28)$$

with $K = R_s/(2G_0 T_S)$. Here, G_0 , T_S are gain coefficient and the sampling frequency.

7 ASYNCHRONOUS MOTOR MODEL

The mathematical dynamic model of the asynchronous motor is described by the equations set [8–11], [13]

$$\frac{dI_{sd}}{dt} = \frac{1}{\sigma L_s} \left[-\left(R_a + \frac{M^2 R_r}{L_r^2}\right) I_{sd} + w_s \sigma L_s I_{sq} + \frac{MR_r}{L_r} \Phi_{rd} + \frac{M}{L_r} w_m \Phi_{rq} + V_{sd} \right], \quad (29)$$

$$\frac{dI_{sq}}{dt} = \frac{1}{\sigma L_s} \left[-\left(R_a + \frac{M^2 R_r}{L_r^2}\right) I_{sq} - \frac{M}{L_r} w_m \Phi_{rd} + \frac{MR_r}{L_r} \Phi_{rq} - \sigma w_s L_s I_{sd} + V_{sq} \right], \quad (30)$$

$$\frac{d\Phi_{rd}}{dt} = -\frac{R_r}{L_r} + (w_s - w_m) \Phi_{rq} + \frac{MR_r}{L_r} I_{sd}, \quad (31)$$

$$\frac{d\Phi_{rq}}{dt} = -\frac{R_r}{L_r} - (w_s - w_m) \Phi_{rd} + \frac{MR_r}{L_r} I_{sq}, \quad (32)$$

$$J \frac{dw}{dt} = T_e - T_r. \quad (33)$$

In this case, the ASM develop an electromagnetic torque T_e expressed as follows

$$T_e = \frac{Mp_p^2}{L_r} (I_{sq} \Phi_{rd} - I_{sd} \Phi_{rq}). \quad (34)$$

d , q axes are corresponding to the synchronous reference frame, L_s , L_r , R_a , R_r and M are — stator and rotor main inductances, resistances and intrinsic self-inductance respectively. J is total inertia, σ dispersion factor. I_{sd} , Φ_{rd} , I_{sq} , Φ_{rq} are d -axis stator current, rotor flux and q -axis stator current, rotor flux respectively. w_s and w_m are the angular speed of the rotating magnetic and electric fields.

AS Motor Characteristics:

$$P = 746 \text{ Watts}, f = 60 \text{ Hz}, I_{sn} = 3.4 \text{ A}, T_e = 5 \text{ Nm}.$$

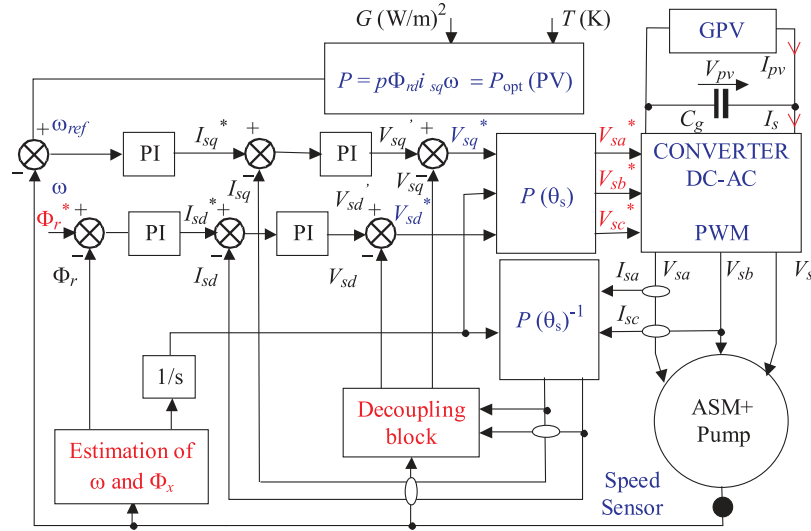


Fig. 6. Block diagram of an ASM vectorial command

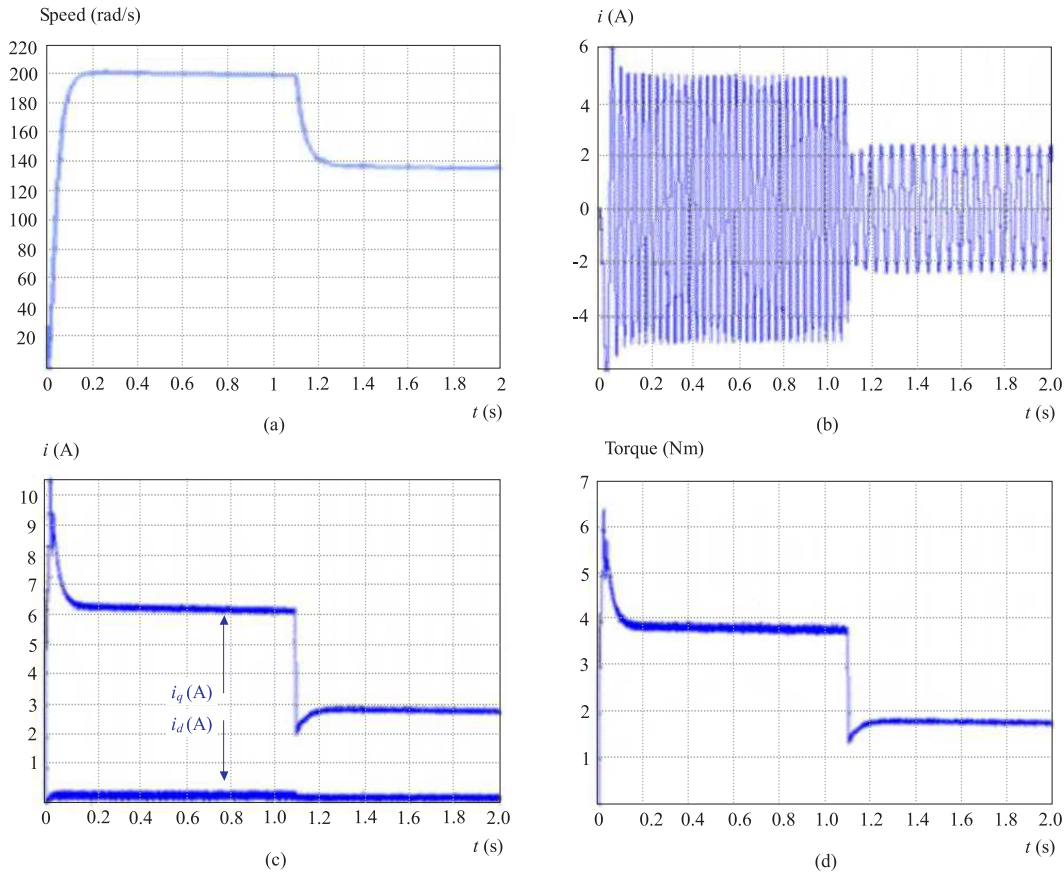


Fig. 7. Simulation results of speed, stator current per phase and motor torque

$R_a = 4 \Omega$, $L_s = 0.3676 \text{ H}$, $R_r = 1.143 \Omega$, $L_r = 0.3676 \text{ H}$, $M = 0.3439 \text{ H}$, $J = 3 \times 10^{-2} \text{ Kg/m}^2$, $p_p = 2$.

PID parameters:

$$T_i = 0.9, K_p = 3.$$

8 GLOBAL SYSTEM

For a damping coefficient, for ASM, $\xi = 1$, and $\omega_n t_{rep} = 4.75$, t_{rep} — representing the response time

of speed, the transfer function for current i_{sd} and i_{sq} of the system in open loop is

$$H(p) = C(p) \frac{1}{R_a(1 + \tau_s p)}, \quad (35)$$

$$C(p) = K_p + \frac{K_i}{p} \quad (36)$$

with $\tau_s = \frac{R_a}{L_s}$, K_i and K_p the proportional-integral parameters.

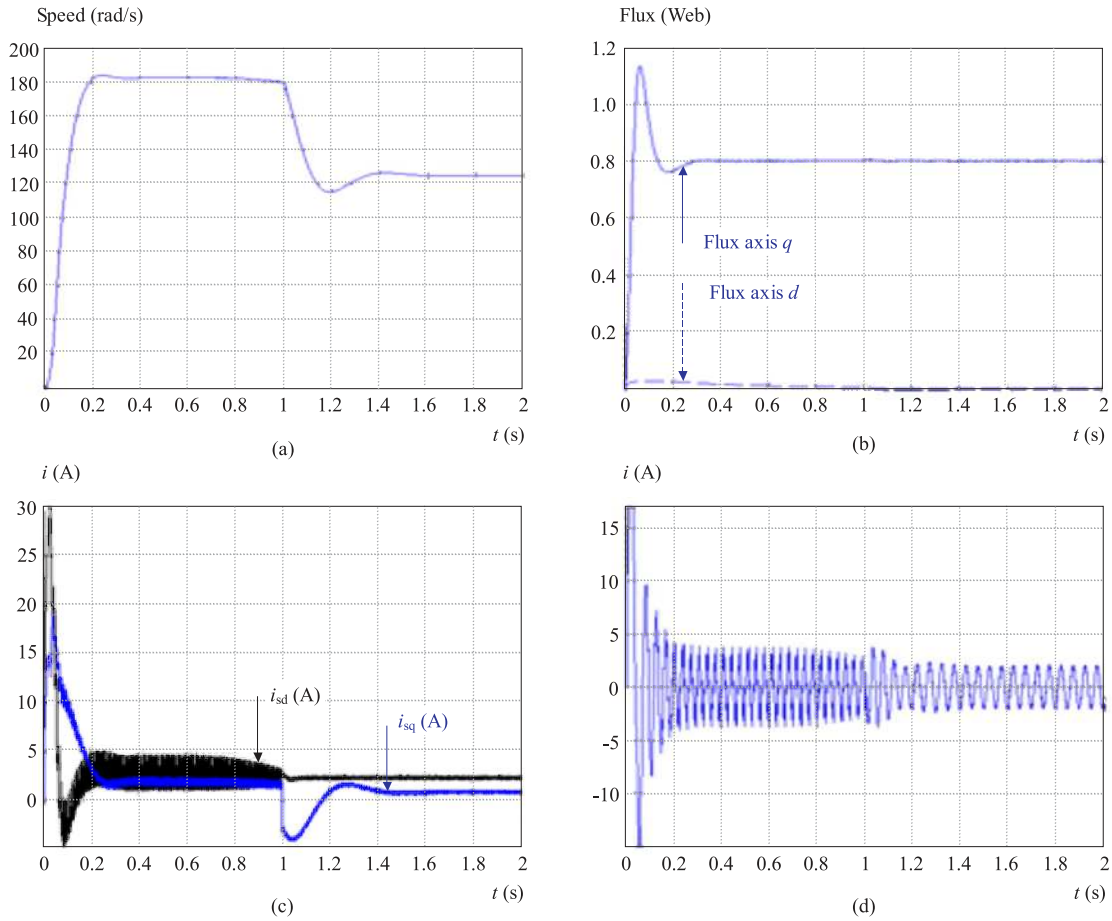


Fig. 8. Simulation results of speed, flux and stator current

9 SIMULATION RESULTS OF THE PMSM

In this section, the simulation results of the optimization of a photovoltaic pumping system fed by electrical synchronous motor coupled with a centrifugal pump are presented

If we apply during every 1 second two levels of solar radiation $G=1000\text{W/m}^2$ and $G=450\text{W/m}^2$, simulation results are carried out to verify the performance of field-oriented control, the system is stabilized on the level of the reference variables.

The first stage of solar radiation corresponding to $G=1000\text{W/m}^2$ at the optimization does not affect the various studied quantities. The speed is about 189 rad/s, the direct stator current value $i_d=0\text{A}$, $i_q=6\text{A}$, the stator current $i_{sa}=3.4\text{A}$, the torque is about 3.95 Nm Fig. 8.

At the second stage of solar radiation corresponding to $G=450\text{W/m}^2$, the optimization affect the various studied quantities. The speed is about 135 rad/s, the value of the direct stator current $i_d=0\text{A}$, $i_q=3\text{A}$, the stator current $i_{sa}=2\text{A}$ and the torque is about 1.98 Nm Fig. 8. The studied various quantities prove the performance of our system.

10 SIMULATION RESULTS OF THE ASM

If we apply during every 1 second two levels of solar radiation $G=1000\text{W/m}^2$ and $G=450\text{W/m}^2$. Simulation results are carried out to verify the performance of field-oriented control, with and without optimization, the flux command is set to $\Phi_{rd}=0.8\text{Wb}$ and $\Phi_{rq}=0\text{Wb}$, see Fig. 9.

The first stage of solar radiation corresponding to $G=1000\text{W/m}^2$, has no effect on the optimization of various studied quantities. The speed is about 180 rad/s, the value of the direct stator current $i_{sd}=3\text{A}$, $i_{sq}=3.2\text{A}$ and the stator current $i_{sa}=3.2\text{A}$.

Also in spite of the step changes in the external load torque, the rotor speed and rotor flux tracking are successfully achieved. It is important to note that, even though the power provided by the photovoltaic generator is lower than its maximum, this result has motivated the use of DC/AC inverter for ensuring the desired maximum power point tracking, which essentially keeps the convergence power at its optimal value.

In order to test the efficiency of the proposed method, we also carried out some simulations when the photovoltaic generator is able to operate around working optimal point.

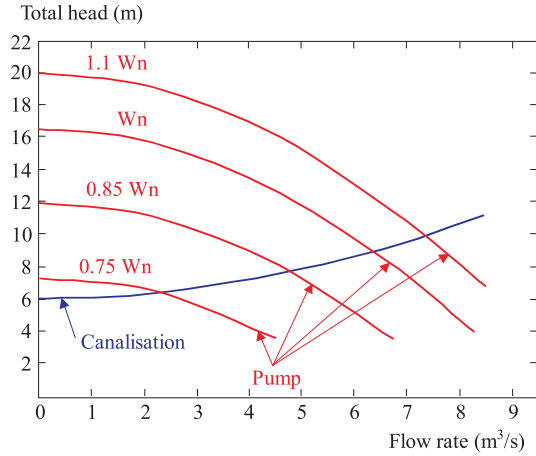


Fig. 9. Flow rate characteristics

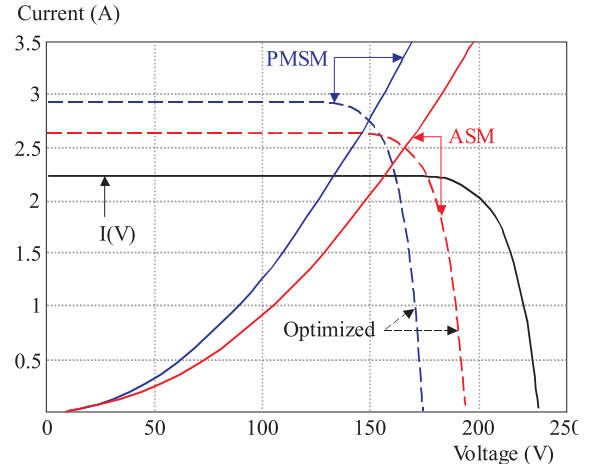


Fig. 10. I-V and Loads characteristics

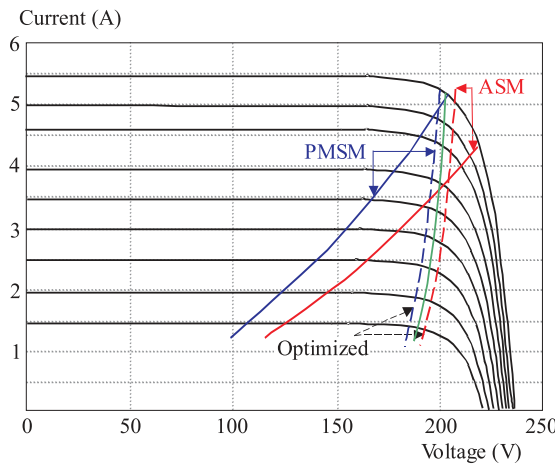


Fig. 11. Operation points of the PV pumping

11 LOCATION OF MAXIMUM POWER POINTS

The generator power is equal to $P_{pv} = V_{pv}I_{pv}$ and the maximum power is obtained for:

$$\frac{P'Y_{pv}}{V'Y_{pv}} = \frac{I'Y_{pv}}{V'Y_{pv}} V_{pv} + I_{pv} = 0. \quad (37)$$

Let I_{mp} be the value of optimal current when power is maximum. By substituting $\frac{I'Y_{pv}}{V'Y_{pv}}$, V_{pv} and I_{pv} by their values in (37), we obtain the following equation:

$$I_{mp} + \frac{(I_{mp} - I_L - I_0) \left[\ln \left(\frac{I_L - I_{mp}}{I_0} + 1 \right) - \frac{I_{mp} R_s}{A} \right]}{1 + (I_L + I_{mp} + I_0) \frac{I_{mp} R_s}{A}} = 0. \quad (38)$$

The solution of the equation (38) by the Newton-Raphson method in motor-pump coupling mode, is governed by the following equation

$$I_{mp} V_{mp} = p \Phi \omega_i \eta_c \eta_m \eta_p. \quad (39)$$

η_c , η_m , η_p , are respectively the inverter efficiency, motor efficiency and pump efficiency.

12 CENTRIFUGAL PUMP MODEL

The head-flow rate $H - Q$ characteristic of a mono-cellular centrifugal pump is obtained using Pleider-Peterman model [14], [15]. The multispeed family head-capacity curves are shown in Fig. 9 and can be expressed approximately by the following quadratic form:

$$h = a_0 w_r^2 - a_1 w_r Q - a_2 Q^2 \quad (40)$$

with a_0 , a_1 , a_2 are coefficients given by the manufacturer. The hydraulic power and the resistive torque are given by,

$$P_H = \rho g Q H, \quad (41)$$

$$C_r = k_r \Omega^2 + C_s. \quad (42)$$

where Q — is the water flow (m^3/s) and H — is the manometric head of the well (m).

Centrifugal pump parameters:

$$\omega_n = 150 \text{ rad/s}, a_1 = 4.923410^{-3} \text{ m}/(\text{rad/s})^2,$$

$$a_2 = 1.5826 \times 10^{-5} \text{ m}/(\text{rad/s}) (\text{m}^2/\text{s}).$$

$$a_3 = -18144 \text{ m}/(\text{m}^3/\text{s})^2,$$

Canalisation parameters:

$$H = 10 \text{ m}, l = 7.4 \text{ m}, d = 0.006 \text{ m}, g = 9.81 \text{ m/s}^2,$$

$$\rho = 1000 \text{ kg/m}^3.$$

13 ILLUMINATION'S INFLUENCE ON WORKING OPTIMAL POINT

While keeping the power generator at constant value, the optimization system improves the motor efficiency which will work around the working optimal point of the generator, Fig. 10.

The optimization system improves the motor efficiency which will work around the working optimal point of the generator; the load motor power characteristic will slip towards the band of the generator maximum powers, which ranges between 180 and 220 volts, for a variable illumination levels between 250 W/m^2 and 1100 W/m^2 , Fig. 11.

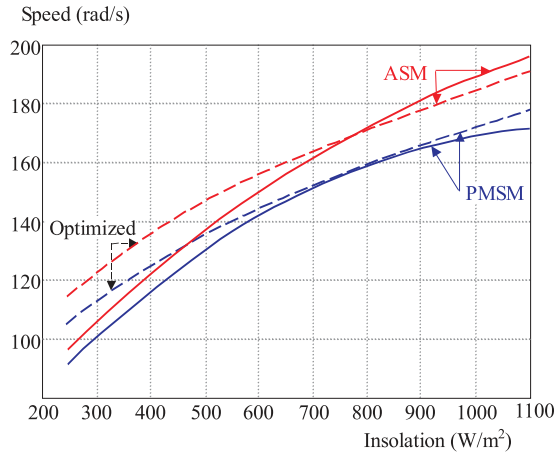


Fig. 12. Speeds of PV pumping driven by PMSM (1) and an ASM (2)

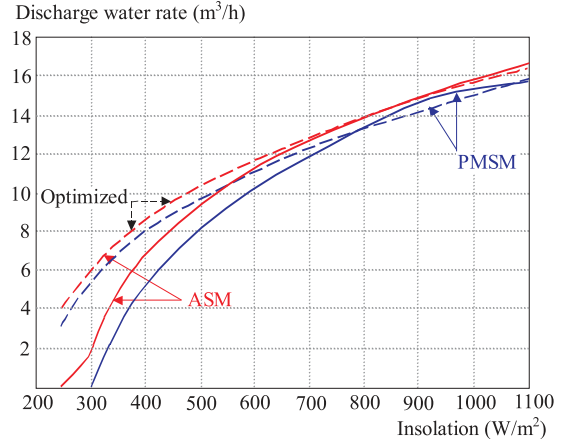


Fig. 13. Flow rate of PV pumping

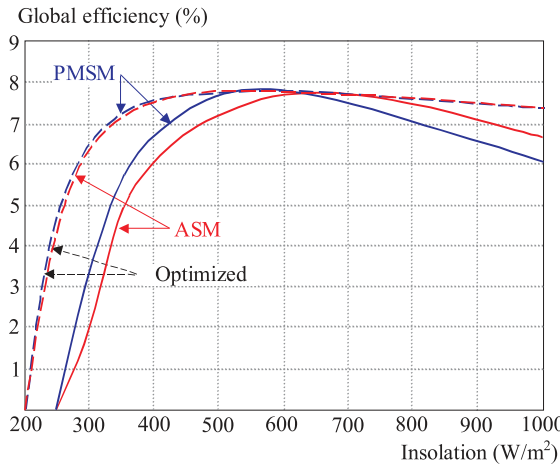


Fig. 14. Global efficiency of PV pumping.

For the direct coupling the driving system motor-pump functions only start from 250 w/m^2 for ASM and 300 w/m^2 for PMSM, contrary to the optimized coupling whose splashing phase ceases starting from 100 w/m^2 , Figs. 13 and 14.

For a temperature $T = 298^\circ\text{K}$, and an illumination $G = 450 \text{ w/m}^2$, the power gain is 49.32 % for PMS Motor and 25.23 % for AS motor, after optimization, it will be 20.12 % for PMSM and 7.35 % for ASM at 900 w/m^2 .

Optimization is better for weak illuminations, until 600 w/m^2 , the global efficiency of the complete system generator, motor-pump being weak, approximately between 7 % and 8 %.

14 CONCLUSION

We showed the principal characteristics of a photo-voltaic system allowing the pumping of water with solar energy. A PV generator outputting on an electronic power inverter detecting the working optimal point is presented. This generator drives a synchronous permanent magnet motor with smooth poles firstly and an induction motor

that by using the vectorial command principle in the reference (d, q) . This method makes it possible to obtain very good performances similar to those of a DC motor, because one obtains an electromagnetic torque directly proportional to the current absorptive by the load.

For achieving better motor torque generating characteristics, the conventional PI controller has been introduced in this paper for the vectorial command of an ASM machine fed by a photovoltaic generator. A current control scheme combining a decoupling control to achieve a fast dynamic response in a field orientation-controlled induction motor drive was presented in this paper. The ASM machine drive with rotor flux, stator current and speed controllers has exhibited good transient and steady-state performance. The results show the flux magnitude has been maintained as constant and a torque exhibits a fast response.

In this paper to take advantage of the field oriented-control, the flux and current controller have been designed using stator and rotor equations in the rotor flux frame since the flux and current controllers have simple forms according to the choice of closed-loops transfer functions, they can be easily designed and implemented. On the other hand, the control of the duty ratio is achieved by using the integral controller. The use of this controller gives good results for the maximum power tracking. A comparative study was carried out on the systems described in Mimouni and al [16] and Duzat [17]. The simulation results show that an increase of both the daily pumped quantity and pump efficiency are reached by the proposed approach. In addition, the generator voltages control law leads to a less expensive and noncomplex implementation. Thus the advantages described are acquired meanwhile overriding their inconvenience.

Nomenclature

| | |
|-------|---|
| q | — Electron charge ($1.9 \times 10^{-19} \text{ C}$) |
| K | — Boltzmann constant ($1.38 \times 10^{-23} \text{ J/K}$) |
| E_g | — Material band gap energy (1.12 eV) |
| V | — Output generator voltage (V) |

| | |
|----------------|---|
| I | — Generator current (A) |
| I_{sc} | — Short-circuit current (A) |
| I_0 | — Reverse saturation current (A) |
| R_S | — Series resistance of PV cell (Ω) |
| R_P | — Parallel resistance of PV cell (Ω) |
| I_{mp} | — Maximum point current (A) |
| V_{mp} | — Maximum point voltage (V) |
| V_{oc} | — Open circuit voltage (V) |
| P_{max} | — Maximum power of PV panel (W) |
| G | — Solar irradiance (W/m^2) |
| $\mu_{V_{oc}}$ | — Temperature coefficient of open-circuit voltage — ($\text{A}/^\circ\text{C}$) |
| $\mu_{I_{sc}}$ | — Temperature coefficient of short-circuit current — ($\text{V}/^\circ\text{C}$) |
| N_{oct} | — Nominal Operating Cell Temperature |
| N_s, N_p | — Number of cells in series and in parallel |
| V_{mot} | — Motor voltage (V) |
| R_{sa} | — Stator resistance per phase (Ω) |
| L_d | — d -axis self inductance of the stator (H) |
| L_q | — q -axis self inductance of the stator (H) |
| M | — Mutual inductance (H) |
| ω | — Motor angular speed (rad/s) |
| ω_s | — Angular speed of magnetic field (rad/s) |
| ω_m | — Angular speed of electric field (rad/s) |
| H | — Total head (m) |
| H_g | — Geodetic head (m) |
| Q | — Flow rate (m^3/s) |
| ρ | — Water volumic mass (kg/m^3) |

REFERENCES

- [1] APPELBAUM, J.—BANY, J.: Performance Characteristics of a Permanent Magnet DC Motor Powered by Solar Cells, *Sol. Energy* **22**, (1979), 439.
- [2] APPELBAUM, J.—SHARMA, M. S.: The operation of permanent magnet dc motors powered by a common source of solar cells, *IEEE Trans. Energ. Convers.* **4** No. 4 (1989), 635–642.
- [3] ROGER, J. A.: Theory of the Direct Coupling between DC Motors and Photovoltaic Solar Arrays, *Sol. Energy* **23** (1979), 193.
- [4] ANIS, W.—METWALLY, H. M. B.: Dynamic performance of a directly coupled PV pumping system, *Sol. Energy* **53** No. 3 (1994).
- [5] BETKA, A.—MOUSSI, A.: Performance optimization of a photovoltaic induction motor pumping system, *Renewable Energy* **29** (2004), 2167–2181.
- [6] HUA, C.—LIN, J.—SHEN, C.: Implementation of a DSP Controlled Photovoltaic System with Peak Power Tracking, *IEEE Trans. Ind. Electronics* **45** No. 1 (Feb 1998), 99–107.
- [7] MULJADI, E.: PV Water Pumping with a Peak Power Tracker using a Simple Six Step Square-Wave Inverter, *IEEE Trans. Industry Applications* **33** No. 3 (May/June 1997), 714–721.
- [8] MIMOUNI, M. F.—DHIFAOUI, R.—BRUDNY, J. F.—ROGER, D.: Field-oriented control of double-star induction machine, *Int journal system of analysis modelling simulation (SAMS)* **37** (2000), 181–202.
- [9] GRELLET, G.—CLERC, G.: *Actionneurs Electriques Principes Modèles Commande*, Eyrolles, 1997.
- [10] BOSE, B. K.: A High performance Inverter — Fed Drive System of Interior Permanent Magnet Synchronous Machine, *IEEE Trns Appl.* **1a-24** (Nov/Dec.1998), 97–997.
- [11] JAHNS, T. M.: Flux — Weakening Regime Operation of an Interior Permanent Magnet Synchronous motor Drive IEEE on IA.
- [12] KIN, J. M.—SUL, S. K.: Speed Control of Interior Permanent Magnet Synchronous motor Drive for Flux Zeaking Operation 3, in *Proc. IEEE IAS Annual: eet mpp.* 216–221, 1995.
- [13] MURPHY, J. M. D.—TURNBULL, F. G.: *Power electronics control of AC motor*, Pergamon Press, 1985.
- [14] HAMIDAT, A.—HADJ ARAB, A.—CHENLO, F.—ABELLA, M. A.: Performances costs of the centrifugal and displacement pumps, pp. 19511954, WREC, 1998.
- [15] MOUSSI, A.—BETKA, A.—AZOUI, B.: Optimum design of photovoltaic pumping system, Leicester, UK, UPEC99; 1999.
- [16] MIMOUNI, M. F.—MANSOURI, M. N.—BENGHANEM, B.—ANNABI, M.: Vectorial command of an asynchronous motor fed by a photovoltaic generator, *Renewable Energy* **29** (2004), 433–442.
- [17] DUZAT, R.: Analytic and experimental investigation of a photovoltaic pumping system, PhD thesis, Oldenburg University 2000.

Received 15 January 2007

Rachid Chenni was born in Constantine, Algeria, in 1957. He received the diploma of electrotechnology engineer in 1983 at the science and Technology University of Oran, Master degree (with honors) in electronics, (1996) and his PhD in Physics Energetic from the University of Constantine in Algeria (2006). Since 1996 he has been an Assistant Professor, at the Faculty of Engineering, University Mentouri of Constantine. His main scientific interests are in the fields of circuit theory and applications and power electronics, also his study is about the photovoltaic systems and their applications.

Laid Zarour was born in Constantine, Algeria, in 1976. He received the diploma of electrotechnology engineer in 2002 at the science and technology of Mentouri University of Constantine, Master degree (with honors) in electrotechnics, (2005). He is currently preparing his doctor studies in renewable energy at the Mentouri University, Constantine, Algeria. From 2005, his main scientific interests are in the fields of circuit theory and applications and power electronics, also his study is about the photovoltaic systems and their applications.

Aissa Bouzid was born in Constantine, Algeria, in 1954. He received the diploma of electrotechnology engineer in 1980 at the science and Technology University of Algiers, Master degree electronics, (1985) and his PhD in Electrotechnology from Orsay University of Paris in France (1994). Since 1996 he has been a Professor, at the Faculty of Engineering, University Mentouri of Constantine. His main scientific interests are in the fields of circuit theory and applications and power electronics, also his study is about the photovoltaic systems and their applications

Abdelhalim Borni was born in Biskra, Algeria, in 1977. He received the diploma of electrotechnology engineer in 2003 at the science and technology of Mohamed Khider University of Biskra, Master degree (with honors) in electrotechnics, (2008). He is currently preparing his doctorat in renewable energy at the Mentouri University, Constantine, Algeria. His study is on the photovoltaic systems and their applications.